Linear noise approximation for oscillations in a stochastic inhibitory network with delay

Grégory Dumont[*]
Physics Department, Ottawa University, Ontario, Canada
and Mind, Brain Imaging and Neuroethics, Royal Ottawa Healthcare, Center for Neural Dynamics, Ottawa University, Ontario, Canada

Georg Northoff[†]
Mind, Brain Imaging and Neuroethics, Royal Ottawa Healthcare, Institute of Mental Health Research, Ottawa, Canada
and Center for Neural Dynamics, Ottawa University, Ontario, Canada

André Longtin[‡]
Physics Department, Ottawa University, Ontario, Canada
and Center for Neural Dynamics, Ottawa University, Ontario, Canada

(Received 12 November 2013; revised manuscript received 14 April 2014; published 7 July 2014)

Understanding neural variability is currently one of the biggest challenges in neuroscience. Using theory and computational modeling, we study the behavior of a globally coupled inhibitory neural network, in which each neuron follows a purely stochastic two-state spiking process. We investigate the role of both this intrinsic randomness and the conduction delay on the emergence of fast (e.g., gamma) oscillations. Toward that end, we expand the recently proposed linear noise approximation (LNA) technique to this non-Markovian "delay" case. The analysis first leads to a nonlinear delay-differential equation (DDE) with multiplicative noise for the mean activity. The LNA then yields two coupled DDEs, one of which is driven by additive Gaussian white noise. These equations on their own provide an excellent approximation to the full network dynamics, which are much longer to integrate. They further allow us to compute a theoretical expression for the power spectrum of the population activity. Our analytical result is in good agreement with the power spectrum obtained via numerical simulations of the full network dynamics, for the large range of parameters where both the intrinsic stochasticity and the conduction delay are necessary for the occurrence of oscillations. The intrinsic noise arises from the probabilistic description of each neuron, yet it is expressed at the system activity level, and it can only be controlled by the system size. In fact, its effect on the fluctuations in system activity disappears in the infinite network size limit, but the characteristics of the oscillatory activity depend on all model parameters including the system size. Using the Hilbert transform, we further show that the intrinsic noise causes sporadic strong fluctuations in the phase of the gamma rhythm.

DOI: 10.1103/PhysRevE.90.012702 PACS number(s): 87.19.lj, 02.30.Oz

I. INTRODUCTION

One of the major challenges in neuroscience is to produce an analytical treatment of variability. It is important to first make the distinction between an internal source of fluctuation and an external one [1,2]. While the external source of noise usually refers to the random fluctuations attributed to the environment of the neurons, the internal source is mainly imputed to the probabilistic nature of the chemical reactions governing the firing process of neurons. More precisely, in a neural network, external or "extrinsic" noise is present because neurons are bombarded by thousands of synaptic inputs, while the internal or "intrinsic" variability refers to the randomness in the openings and closings of the ion channels underlying action potentials [3].

For the description of a neural network, once the deterministic equation that describes the mean activity is written, noise is usually included to obtain a stochastic differential equation of the Langevin type (see, e.g., [4]). This equation can then be further analyzed via the Fokker-Planck equation. Here, however, we wish to understand the contribution of a special form of intrinsic fluctuations to the dynamics of neural networks by considering a two-state (quiescent versus active) probabilistic formulation of the single neuron dynamics. Among other things, this formal approach leads to system-size-dependent effects; note that this is not a necessary condition for such effects, since, e.g., they are known to occur even in deterministic networks with chaotic dynamics [5]. As we will show, this two-state probabilistic approach can also accommodate the inclusion of delays. Thus, we investigate a model where the variability is only treated intrinsically as in [6,7]. Although this form of noise finds its origin in single neurons, it is propagated through the network such that ultimately each neuron experiences its intrinsic noise plus an extrinsic noise coming from the synaptic interactions with the other cells.

It is well established that random fluctuations alter considerably the nature of a dynamical system. As a basic example, noise produces stochastic oscillations that we do not see in the deterministic dynamics. For the treatment of the internal fluctuation, examples can be found in the context of predator-prey population dynamics [8] or epidemics [9]. In those situations, random fluctuations transform the damped oscillatory system into a system with noise-induced oscillations. The long-term behavior is no longer a convergence toward a

[*]gdumont@uottawa.ca
[†]georg.northoff@theroyal.ca
[‡]alongtin@uottawa.ca

stable equilibrium. From a mathematical perspective, a precise description is that the eigenvalues of the stability matrix are complex (and of course conjugate). This kind of oscillatory behavior is often referred to as a quasicycle. Furthermore, because the variability is purely intrinsic, an important feature of these oscillations is that the amplitude depends on the size of the system considered [8,9].

In computational neuroscience, similar observations were reported, using a standard cortical model of a neural network composed of excitatory-inhibitory cells [6,7] [the E-I interaction, also called the PING model for a pyramidal-interneuron network for gamma oscillation (30–100 Hz)]. In the presence of internal fluctuations, stochastic oscillations were observed numerically and explained analytically. The deterministic activity of the neural network, computed by averaging the mean activity of the pyramidal and of the inhibitory neurons, approaches a fixed point in an oscillatory fashion. Nonetheless, the fluctuations lead the system to a persistent oscillatory behavior. In this situation, the intrinsic variability transforms deterministic damped oscillations into noise-induced oscillations. Again, the eigenvalues of the stability matrix are complex conjugate. Furthermore, the power spectrum of the global activity agrees well with the power spectrum of local field potential (LFP) recordings [10]. So while oscillations are ubiquitous in the brain, and there is ongoing debate about how they are generated (see, e.g., [11] for a review on gamma oscillations), this phenomenon where oscillations are induced by intrinsic noise adds another plausible explanation of gamma oscillations present in the cortex [6].

Another well understood mechanism involves the coherent activity generated solely by excitatory neurons (the E-E interaction—see [12–14]). In this situation, all the neurons emit their action potential at the same time, creating a burst in the firing rate. We refer the interested reader to [7] for the consequences of the internal variability on such a pyramidal cell network.

On the other hand, oscillations induced by the conduction delay of the inhibitory feedback (the I-I interaction, also called the ING model) are another possible mechanism—see [15] and [4] for theoretical and computational models, and see [11] for a biophysical description. For this latter modeling hypothesis, the effect of intrinsic variability as defined above (i.e., probabilistic two-state neurons) has not been investigated, because Refs. [15] and [4] deal with deterministic integrate-and-fire neurons driven by synaptic input in the diffusion approximation (i.e., with additive Gaussian white noise on the current balance equation). Those studies enable the investigation of the influence of the intensity of this noise on network dynamics, as well as an approximate treatment of the problem posed by the presence of both Gaussian white noise and delay. Actually, due to the non-Markovian nature of such a process, the conduction delay is usually ignored in theoretical studies. However, the combination in neural networks of intrinsic noise and delay has not received attention, and its analysis follows below. We also note that the intrinsic variability of inhibitory interneurons (with blocked synaptic inputs) has recently been proposed as a major source of cortical variability [16].

A large class of (deterministic) delay differential equations (DDEs) is well known to possess a Hopf bifurcation from a fixed point to a purely oscillatory solution; the associated characteristic equation for the stability analysis then generally admits an infinite number of complex-conjugate roots. The interested reader may find in [17] a variety of applications of DDEs to biology. In addition, DDEs are highly sensitive to noise; see [18]. In fact, extrinsic noise, producing a delayed Langevin equation, has been shown numerically and experimentally to induce oscillations in the human pupil light reflex [19].

Our aim here is to extend the existing result on the finite-size "intrinsic" stochastic effects already noted on the Wilson-Cowan model [6,7] to a network of inhibitory cells with intrinsic noise and conduction delays. The main question we ask is as follows: do similar stochastic oscillations due to a finite-size effect occur if the oscillations are caused by an inhibitory delayed feedback? And if so, can they be treated analytically by the linear noise approximation formalism?

The present work is organized as follows. We first formulate the dynamics of a finite number of connected interneurons (I-I interaction) using similar ideas to those for the E-I interaction network in [6] or the E-E interaction in [7]. The stochastic spiking model is written such that the deterministic rate equation (see [20] for example) is recovered when the network is infinitely large. With the help of recent mathematical techniques [21,22], we deduce in the second part a nonlinear stochastic delay differential equation that characterizes the activity. Using the linear noise approximation, we are able to compute an approximation of the power spectrum that is in good agreement with the spectrum obtained numerically by averaging over realizations of the intrinsic noise. We then discuss how the delay and the intrinsic variability induce oscillations even if the deterministic counterpart does not exhibit oscillations. We also illustrate how the intrinsic noise causes strong sporadic fluctuations in the phase of the gamma rhythm. We end the paper with a conclusion section, and we discuss future perspectives resulting from our work.

II. STOCHASTIC SPIKING MODEL

In this section, we expose in detail the stochastic spiking model. In neuroscience, a pioneer work taking into account the stochasticity imputed to a finite-size effect can be found in [23]. For the sake of clarity, we adopt a notation similar to that of [6] and [24]. The network is assumed to consist of N inhibitory cells (I-cell). Each cell is characterized by a random walk between two possible states (active or silent). When the neuron enters in the active state, the cell is said to fire an action potential. The transition rates from one state to another are chosen such that the rate model (see [20], for example) is recovered in the mean-field limit. During a short interval of time $(t,t+dt)$, the probability that a neuron jumps from the active state to the silent state is αdt (see Fig. 1), with α representing the (usually very fast) decay rate of the active state of the neuron back to the quiescent state. In other words,

$$\mathcal{P}(\text{active} \to \text{quiescent}, \text{during } dt) = \alpha dt.$$

In the other direction, from quiescent to active, things depend on the synaptic input s the neuron receives. The probability to jump from the quiescent state to the active state is calculated

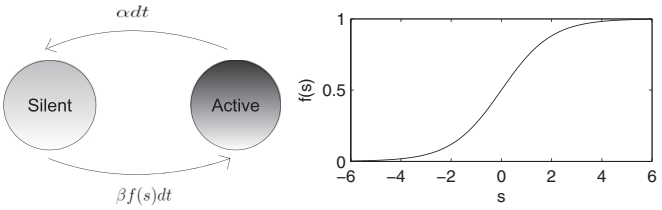

FIG. 1. The left panel is a schematic representation of the random walk between the two possible states (active and quiescent). During a short interval of time $(t,t+dt)$, a neuron that is in the active state has probability αdt to jump into the quiescent state, and similarly, a probability $\beta f(s)dt$ to jump from the quiescent state into the active state, where f is the response function (1) and s is the synaptic input. The right panel is a graphical representation of the response function f.

using the response function f in Fig. 1):

$$\mathcal{P}(\text{quiescent} \to \text{active}, \text{during } dt) = \beta f(s)dt,$$

where the response function f is

$$f(s) = \frac{1}{1+e^{-s}}. \tag{1}$$

Let $l(t)$ denote the integer number of active neurons at time t, which we will also interchangeably call the network activity or the global activity. Assuming an all-to-all coupling, the synaptic input that a neuron receives is

$$s(t) = h - wl(t-\tau)/N,$$

with h the external influence upon the network (a deterministic parameter), w the synaptic strength, and τ the axonal conduction delay. Note that, while this input $s(t)$ is here called "synaptic," it is still considered intrinsic rather than external, since it originates solely from the two-state probabilistic transitions in each neuron. Recent work that has expanded this description (in the zero-delay context) to include both intrinsic and extrinsic noise at this step can be found in [25]. Notice also that the model is built under the assumption that the network is perfectly homogeneous.

Following the important remark in [24], we chose in all our simulations $\alpha = 0.1$, which corresponds to a time scale of $\alpha^{-1} = 10$ ms (1 ms for the action potential plus 9 ms for the refractory period). Such a value mimics the refractory period even if the refractoriness is not explicitly modeled. In our simulation, we took delays in the range of the cortico-cortical axonal conduction delay of a monkey [26].

We now illustrate the dynamics of the model with numerical simulations. We show in the upper part of Fig. 2 some raster plots depicting the spiking time of each neuron. The simulation presented in Fig. 2 illustrates the oscillatory behavior of the global activity. This is confirmed by the lower plots of Fig. 2, which show the power spectrum of the global activity. The power spectrum is computed numerically by an averaging of many different realizations of the stochastic process. Furthermore, the power spectrum is estimated after discarding the transient dynamics that depend on the initial state. As we see in Fig. 2, the power spectrum exhibits multiple resonance peaks. The dominant frequency is in the gamma band.

To get a better understanding of the kind of gamma oscillation the model induces, we computed in Fig. 3 the phase via a Hilbert transform (top panel) and the instantaneous frequency from this Hilbert phase (bottom panel) using the method in [27]. Toward that end, we have assumed formally that the global activity can be written as

$$l(t)/N = \langle l(t)/N \rangle + E(t)\cos\theta(t).$$

The phase $\theta(t)$ can be extracted using the Hilbert transform of the activity on the left-hand side from which the mean of this activity (first term on the right-hand side) has been subtracted. The computation of the instantaneous frequency is normally

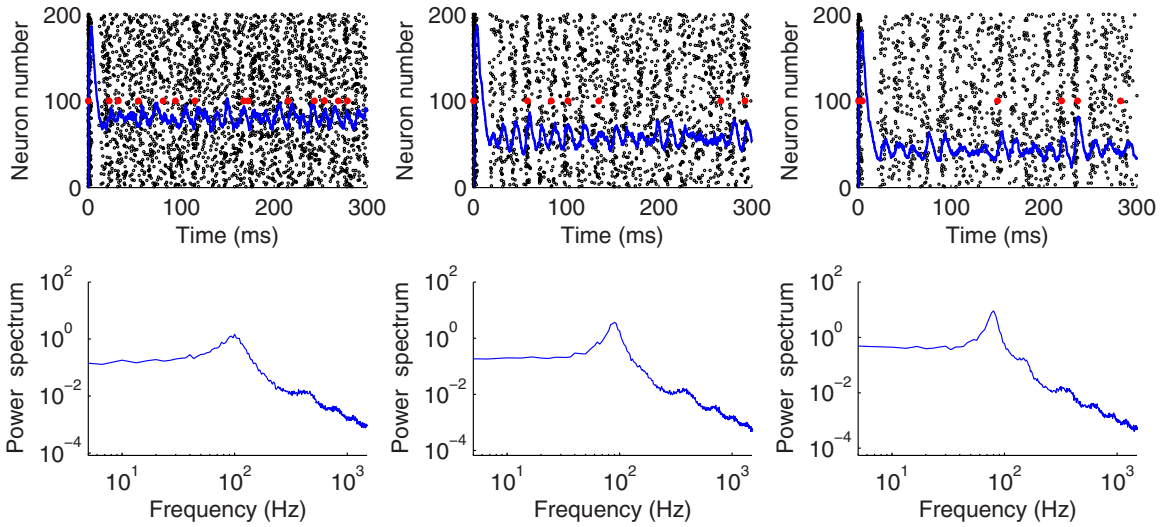

FIG. 2. (Color online) Effect on the network of the conduction delay τ and the synaptic strength w. The top panels are raster plots of 200 interneurons. The blue line represents the global activity $l(t)$ of the network. We show in red the spike train of one particular neuron. The bottom panels show the power spectrum of the global activity, computed by averaging over 100 realizations. The parameters for all simulations are $\alpha = 0.1$, $\beta = 2$, and $h = 0.3$. Further, $\tau = 3.7$ ms and $w = 9$ for the left simulation, $\tau = 4.2$ ms and $w = 15$ for the middle simulation, and $\tau = 4.7$ ms and $w = 22$ for the right simulation.

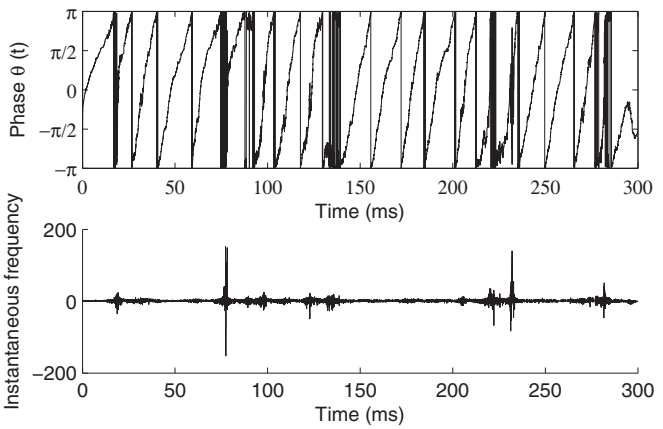

FIG. 3. Study of the phase of the oscillatory network. The top panel shows the evolution in time of the phase computed via the Hilbert transform of the global activity $l(t)$. The bottom panel shows the instantaneous frequency referenced to the mean frequency. The parameters for the simulation are $\alpha = 0.1$, $\beta = 2$, $h = 0.3$, $\tau = 3.5$ ms, and $w = 18$.

given by a discretized version of

$$\omega(t) = \frac{d}{dt}\theta(t).$$

Note that since the phase is discontinuous when it increases by 2π, special precautions are needed to compute the derivative. This is achieved using the more rigorous definition in [27], Eq. (43). Since in our case the system has a dominant frequency that on average moves the phase forward in time, one would expect that the phase is approximately given by $\theta(t) = \omega_0 t + p(t)$. The quantity $p(t)$ can be interpreted as phase fluctuations of the stochastic oscillatory process. When the phase is regular (i.e., increasing close to linearly), the instantaneous frequency is almost constant, while when a phase fluctuation occurs, the instantaneous frequency increases or decreases. Consequently, the estimated instantaneous frequency takes on positive values as well as negative values since the noise can cause phase advances or delays with respect to the mean

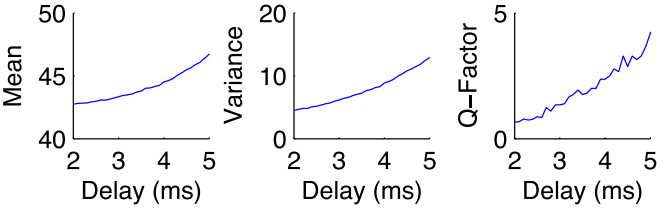

FIG. 5. (Color online) Study of the mean, variance, and Q factor of the global activity $l(t)$ as a function of the conduction delay. The parameters for the simulation are $\alpha = 0.1$, $\beta = 2$, $h = 0.3$, and $w = 22$.

phase. Interestingly, Fig. 3 illustrates that the phase of the gamma cycle is highly variable and exhibits sporadic strong fluctuations. Similar observations were reported with LFP data [28].

The upper plots of Fig. 4 give the interspike interval (ISI) distribution. We see that the neurons are almost Poissonian for the left simulation. The ISI histogram looks bimodal for the middle, and is clearly multimodal for the right panel. We will relate this behavior to the bifurcation (i.e., the threshold for the onset of oscillatory behavior) in the following section. Similar observations were reported in [24] (without delays).

To further investigate the impact of conduction delay on the oscillatory behavior, we have computed the mean of the global activity with respect to the delay in the first panel of Fig. 5. Interestingly, in this stochastic two-state process, the mean activity does depend on the delay. A larger conduction delay induces a higher mean activity. We have also computed the Q factor of the peak, which is a quantitative measure of the strength of the resonant behavior. This factor was defined here as the width of the spectral peak at 80% of its maximal value, divided by the frequency at which the peak occurs. We have found that the variance of the activity as well as the Q factor of the power spectrum increase with the delay, as illustrated in Fig. 5.

Closer inspection reveals that a higher value of w or τ leads to a smaller mean activity. Indeed, we will see below that increasing the parameters τ and w also brings the system

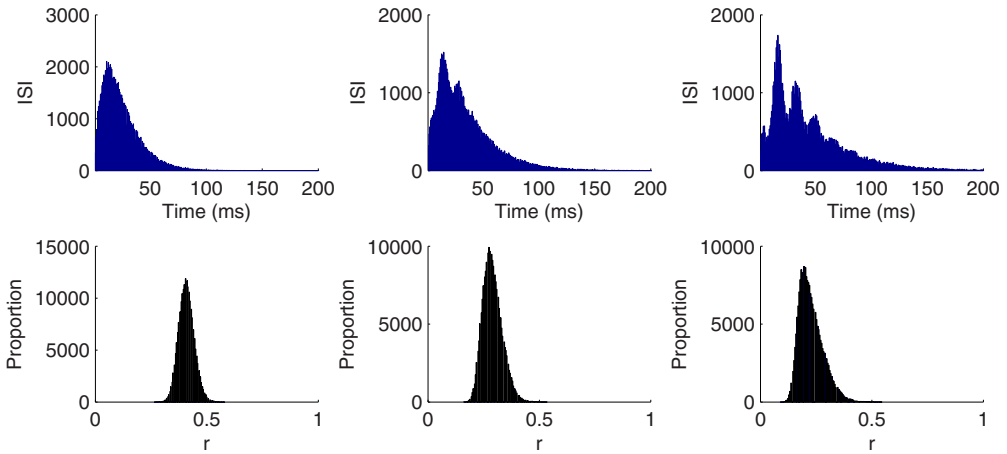

FIG. 4. (Color online) Effect on the network of the conduction delay τ and the synaptic strength w. The top plots show the interspike interval distribution. The bottom panels show the distribution of the global activity $l(t)$. The parameters are those for the three simulations presented in Fig. 2.

closer to the threshold for deterministic oscillations. Indeed, coming back to the first plot (the raster plot), we show with red spots the spiking times of one particular neuron. As one can see, a given neuron does not spike in each gamma cycle, but often misses several cycles before spiking again (this is also seen in LIF models—see [15]). More surprisingly, the neuron can sometimes fire twice in the same cycle. Similar observations were reported in [24].

We also show in the lower plots of Fig. 4 the distribution of the mean activity. This activity is clearly unimodal and even looks Gaussian for all parameters investigated, in spite of the fact that the interval histograms exhibit an oscillatory envelope near and above the bifurcation.

As noticed in [6], a stochastic model of oscillations has the advantage of enabling a calculation of the complete power spectrum, rather than just the peak frequency, which makes possible the comparison with experimentally obtained spectra. We refer the interested reader to [10] for some comparison with local field potential data.

In the following sections, to get a clear picture of what causes the oscillations, we make a formal link between the stochastic spiking model and a noisy rate model. Using the linear noise approximation, we will separate the deterministic properties from the random fluctuations. The latter allow us to compute an approximation of the power spectrum that predicts the oscillations of the activity in terms of the model parameters.

III. LINK TO A STOCHASTIC RATE MODEL

To clarify the dynamics observed in Fig. 2, diverse approaches can be taken. In [23] and [29] (see also [30] for other spiking models), the authors choose a path-integral representation of the stochastic process. In this article, we do not follow this approach. We focus our analysis instead on finding an approximation of the power spectrum as in [8] or in [9]. To do so, we link the model to a stochastic rate equation. However, instead of using the master equation formulation, we use recent techniques successfully applied in [21] for chemical reactions and for the Wilson-Cowan model [6]. Introducing the new mean activity variable $r(t) = l(t)/N$, representing the fraction of active neurons, one obtains (see Appendix A 1) that the dynamics of $r(t)$ is described by the nonlinear stochastic DDE,

$$\frac{d}{dt}r(t) = -\alpha r(t) + [1 - r(t)]\beta f[s(t)] + \sqrt{\frac{\alpha r(t) + [1 - r(t)]\beta f[s(t)]}{N}}\eta(t), \qquad (2)$$

where η is a Gaussian white noise,

$$\langle \eta(t) \rangle = 0, \quad \langle \eta(t)\eta(t') \rangle = \delta(t - t'),$$

and $s(t)$ is the synaptic input,

$$s(t) = h - wr(t - \tau).$$

In Fig. 6, we show a schematic representation of the dynamics given by (2). Notice that, taking formally the number of cells N in (2) to be infinitely large, we recover the deterministic rate model, with several applications as exposed in [20]. One potential limitation of the deterministic model is that it only takes into account the mean activity and thus does not give any higher-order statistics. Furthermore, it is well established that random fluctuations may change drastically the dynamics of a system. As we will see later, the deterministic rate equation alone fails in explaining the oscillatory behavior reported in Fig. 2. In what follows, we push further the analysis of (2). To do so, we use the linear noise approximation (LNA) to separate the deterministic and the noisy part.

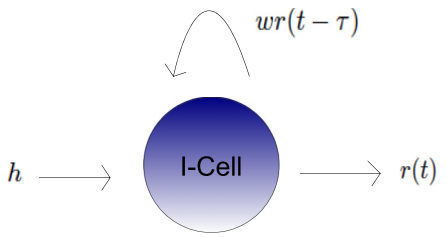

FIG. 6. (Color online) Schematic representation of the inhibitory network. The network is characterized by the synaptic strength w, the axonal conduction delay τ, and by the external influence h.

In our situation, the LNA consists of separating the stochastic and the deterministic part in (2) through a linearization (see [22] for a recent perspective on the LNA). The LNA is not appropriate all the time. For example, when the deterministic rate exhibits two stable states, the linear noise approximation will fail in capturing the transitions between these states (see [7,31]). While the LNA is not relevant for this kind of situation, it is pertinent if the deterministic equation is close to a Hopf bifurcation. In this case, the eigenvalues of the stability matrix are complex conjugate with a real part near the imaginary axis. Then the mean activity converges toward its equilibrium in an oscillatory fashion. The damping effect due to the real part of the eigenvalue will be destroyed by the variability, and will give birth to a quasicycle. This can be seen in [8,9] in the context of population dynamics, and in [6,7] for theoretical neuroscience.

IV. LINEAR NOISE APPROXIMATION

In our situation, the LNA states that the number of active neurons can be approximated by the sum of a deterministic and a stochastic process. Furthermore, the fluctuation part is scaled by a factor $1/\sqrt{N}$ coming from the Van Kampen system size expansion. More specifically (see Appendix A 2), we have

$$r(t) = r_0(t) + \frac{1}{\sqrt{N}}\xi(t),$$

with $r_0(t)$ the deterministic part and $\xi(t)$ the stochastic part. The deterministic part obeys the exact rate model

$$\frac{d}{dt}r_0(t) = -\alpha r_0(t) + [1 - r_0(t)]\beta f[s_0(t)], \qquad (3)$$

with the synaptic current given by

$$s_0(t) = h - wr_0(t - \tau).$$

After algebraic manipulations, including a linearization that keeps only the first-order term in $1/\sqrt{N}$, we found that the

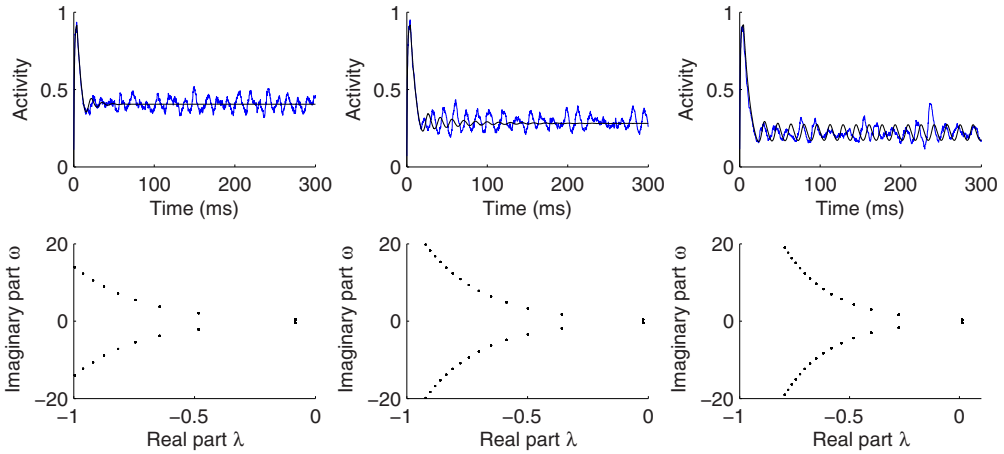

FIG. 7. (Color online) Network simulations and spectral properties. Comparison between the global activity of the stochastic process (blue curve) and the deterministic process (black curve). The figures show the evolution in time of the activity $r_0(t)$ for the deterministic rate model (3) compared with the response of the finite population. If in the two first panels the deterministic rate reaches an equilibrium given by (A5) after oscillating, the finite stochastic population continues oscillating. The parameters for the simulation from left to right correspond to parameters in Fig. 2. For each simulation, we also show the eigenvalues of the characteristic equation (see Appendix A 3). All the eigenvalues are complex conjugate with a negative real part when the stationary state is stable. The rightmost pair of eigenvalues is to the left of the imaginary axis for the left and center panels, while it has crossed the imaginary axis in the case above the Hopf bifurcation illustrated in the right panel.

fluctuation part obeys the linear stochastic DDE,

$$\frac{d}{dt}\xi(t) = -\alpha\xi(t) - \beta f[s_0(t)]\xi(t) - [1 - r_0(t)]\beta f'[s_0(t)]w\xi(t-\tau) + \sqrt{\alpha r_0(t) + [1 - r_0(t)]\beta f[s_0(t)]}\eta(t), \quad (4)$$

where $\eta(t)$ is again a Gaussian white noise. Note that the coefficients of the DDE (4) depend on the solution of the deterministic DDE (3). Together these equations form a system of two DDEs, one of which is linear and driven by additive Gaussian white noise; however, both the drift and diffusion parts are time-dependent.

We report in Fig. 7 a comparison between the deterministic rate (black curve) and the stochastic process (blue curve). In the first two plots, the curves differ in their asymptotic activity, as mentioned in the context of Fig. 2. The agreement of the deterministic rate with the simulations is excellent at all times, including during the initial damped oscillations. Note that the initial conditions for these simulations is quiescence for all neurons. The network activity quickly jumps up from zero, and then undergoes damped oscillations.

As one may also notice from the first two plots, after oscillating, the deterministic part converges toward its equilibrium. The last plot shows a persistent oscillatory behavior also for the deterministic process. Indeed, a stability analysis (see Appendix A 3) shows that (3) is on the stable fixed point side of the Hopf bifurcation. This steady state is the unique fixed point and it is stable. This is due to the fact that the eigenvalues of the stability equation all have a negative real part. For each simulation, we display the eigenvalues in Fig. 7. We present in Fig. 8 the stability boundary for two ranges of parameters. The blue stars stand for the parameters chosen in our simulations. The deterministic rate is thus in a nonoscillatory regime for the first two simulations, and in the oscillatory regime for the last simulation.

Taking into account only the deterministic component is not sufficient for the explanation of the oscillations observed in Fig. 2. It clearly reveals that, under the Hopf bifurcation, both the internal fluctuation and the delay are necessary for an oscillatory regime, although none of them taken separately induces the oscillations. In the next section, we study the stochastic part of the dynamics.

V. POWER SPECTRUM

To compute an approximation of the power spectrum, we assume that the deterministic part of the rate model (3) tends toward its equilibrium. In other words, we assume the deterministic rate to be below the bifurcation point, as was the case in the two first simulations presented in Fig. 2. Then, discarding the transient dynamics, the DDE (4) becomes

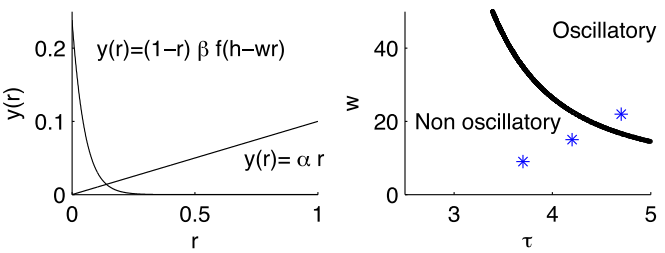

FIG. 8. (Color online) The left panel illustrates the steady state. The stationary state of the deterministic part of the model is a solution of Eq. (A5). The steady state is unique and given by the intersection of an increasing and a decreasing curve. The parameters are $w = 20$, $\alpha = 0.1$, $\beta = 2$, and $h = -2$. The right panel is the bifurcation diagram of the deterministic rate equation (see Appendix A 3). It shows two different regions corresponding to an oscillatory and a nonoscillatory regime. The three asterisks in the right panels correspond to the parameters of the three simulations presented in Fig. 2.

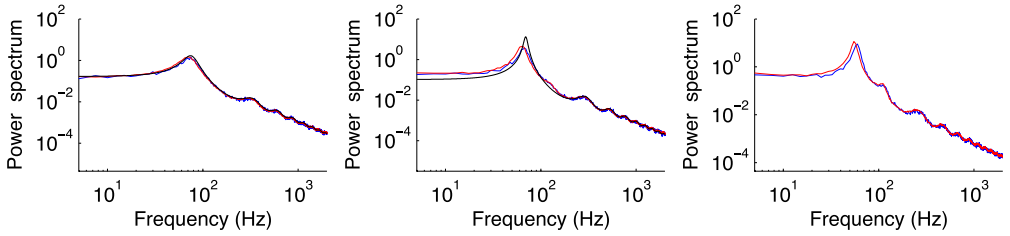

FIG. 9. (Color online) Comparison of the theoretical power spectrum (black curve) given by the mathematical expression (5), the power spectrum from simulations of the full network (blue curve) obtained by averaging 100 trials, and simulations of the SDDE (2) shown in the red curve (again averaging over 100 trials). The parameters for the simulation from left to right correspond to the parameters in Fig. 2.

autonomous, and we can compute its power spectrum. After algebraic manipulations (see Appendix A 4), we found that the power spectrum of the global activity $S(\omega)$ computed numerically in Fig. 2 can be approximated by

$$S(\omega) = 2\pi \bar{r}_0^2 \delta(\omega) + \frac{1}{N} \frac{2\alpha \bar{r}_0}{|\ \alpha + \beta f(\bar{s}_0) + i\omega + w\alpha \bar{r}_0 [1 - f(\bar{s}_0)] e^{-i\omega\tau}\ |^2}, \tag{5}$$

where $\bar{r}_0$ and $\bar{s}_0$ are, respectively, the stationary activity and the stationary synaptic input (see Appendix A 2), and $\delta(\omega)$ is the Dirac measure.

We show in Fig. 9 a comparison between the theoretical power spectrum (black curve) and the power spectrum obtained in Fig. 2 from numerical simulations of the full network (blue curve). As we can see, the theoretical power spectrum (5) obtained from the LNA is in good agreement with the power spectrum obtained through numerical simulation of the network. The formula in fact provides a good explanation of the resonances seen in Fig. 9 in the power spectrum computed from simulations of the network. We carried out the comparison for more simulations than are shown here, and our results hold over a wide range of parameters. We note that there is a discrepancy between theory and numerics mainly at lower frequencies, as was also observed in [6] in the non-Markovian case. This discrepancy increases as the bifurcation is approached from below.

Figure 9 also shows a comparison of the spectra from the theory and the full network simulations with that computed on numerical simulations of the stochastic delay-differential equation (2) (in red). The spectra computed from this SDDE agree very well with the spectra from the whole network for all the regimes shown. There is again a discrepancy at low frequencies that increases as the bifurcation is approached, but it is much smaller than the discrepancy seen with the theoretical spectrum. Thus the SDDE can be used to provide an accurate picture of the spectral properties without having to resort to the much longer full network simulations.

After algebraic manipulations, we find that the local extrema in the spectrum are solutions of the nonlinear equation:

$$\frac{\omega}{\alpha + \beta f(\bar{s}_0)} = -\tan \omega\tau.$$

The latter formula provides good insight into the location of the first frequency peak that is illustrated in Fig. 10. Indeed, it is clear from the equation above that increasing the conduction delay τ should reduce the dominant frequency of the network. In other words, a larger delay leads to a slower gamma oscillation. Further, according to the second panel of Fig. 10, increasing the delay also results in an increase in the amplitude of the peak in the power spectrum of the oscillation. Note that in Fig. 10, when the delay goes to zero, the spectral peak amplitude asymptotically also goes to zero. Nonetheless, the peak amplitude is never exactly zero, and the peak frequency is thus still well-defined numerically.

VI. DISCUSSION

Stochastic oscillations, also known as quasicycles, have received increased attention in the past few years. It is well known, for example, that random fluctuations can generate oscillations not seen in the deterministic dynamics. Recent research has focused in particular on the role of intrinsic variability in the emergence of quasicycles. Examples can be found in ecology as well as in population dynamics [8,9]. This internal variability is imputed to the finite-size effect and can be treated via van Kampen's system size expansion.

Even more recently, in the neuroscience domain, similar conclusions arose. Indeed, in the presence of internal fluctuations in the Wilson-Cowan model, stochastic oscillations were detected numerically and elucidated analytically [6,7]. From a purely mathematical point of view, this is related to the presence of complex-conjugate eigenvalues of the stability matrix of the dynamical system.

However, none of these analyses in neuroscience and population dynamics has considered the presence of delays. Since delay-differential equations also have a stability characteristic equation with complex-conjugate roots, our goal was to extend existing results on the finite-size stochastic effects to a network of inhibitory interneurons with conduction delay, the latter

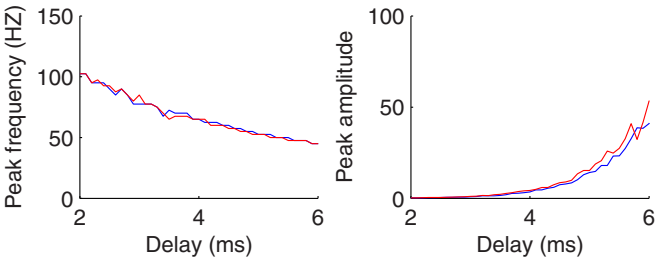

FIG. 10. (Color online) Study of the spectral peak frequency as a function of the delay. The blue curve is for the direct simulation of the stochastic process, and the red curve is for the simulation of the SDDE (2). The parameters are $\alpha = 0.1$, $\beta = 2$, and $h = 0.3$.

giving the dynamics a non-Markovian character. This offers an analytical tool to investigate noise-induced brain rhythms, such as in the gamma range for the parameters of interest in this paper.

To do so, we applied some recent mathematical tools that have been successfully employed in [21] for the modeling of chemical reactions as well as in computational neuroscience [6]. These tools (see also [22]) allowed us to establish a rate equation that keeps track of intrinsic fluctuations. Thus the model can be seen as a noisy version of the standard rate equation (see [20]) in which the stochasticity is treated intrinsically. Furthermore, even if the simulations show persistent oscillations, the network considered here does not develop any persistent oscillatory behavior in the deterministic limit, i.e., it is operated below the Hopf bifurcation.

To get a better understanding of this oscillatory behavior, we computed an approximation of the power spectrum of the global activity via the linear noise approximation. Our analytical finding shows very good agreement with numerical simulations, except when we are too close to the bifurcation threshold. Further, an important feature of the model is that below the bifurcation, neither the noise nor the delay taken separately may cause the oscillatory behavior: the network's propensity to oscillate depends on both the internal variability and the conduction delay.

It is worthwhile to also situate our contribution in the context of two other recent network formalisms that have included delays. The seminal paper in Ref. [15] considered the transition between stationary and oscillatory global activity in both the infinite- and finite-size limits for sparsely connected inhibitory networks. It assumed that the firing rate of each neuron is low compared to the inverse of the membrane time constant, and that each neuron receives a large number of small inputs during that time constant, which enables the approximation of synaptic input by additive Gaussian white noise. Application of the Fokker-Planck formalism leads to a reduced equation for deviations of the global activity around the stationary firing rate, which basically describes a stochastic supercritical Hopf bifurcation. Determination of the two coefficients in that equation is possible after very complex calculations, which include the effects of the delay. Their main quantity of interest is the autocorrelation of the global activity, which shows damped oscillations below the bifurcation, corresponding to noise-induced oscillations. Larger delays lead more readily to oscillatory behavior, as in our case.

The linear-response theory formalism proposed in [4] begins with a previously calculated single neuron susceptibility function, computed using a nonstationary Fokker-Planck analysis of a single LIF neuron with additive Gaussian white noise. That complex calculation describes how the stochastic firing rate is modulated as a function of the frequency of a sinusoidal input. This susceptibility is then incorporated into a linear-response formalism, where inputs are seen to perturb the spontaneous activity. There are no conditions on the connectivity. Rather, the main assumption is that the noise is sufficient to cause a linearization of the single neuron transfer function, i.e., to obtain a good approximation to the susceptibility function. Also, a linear ansatz is made where a stochastic system, governed by nonlinear dynamics and internal noise, is perturbed by external noise and feedback. The formalism enables the computation of single neuron and population spike train power spectra for arbitrary input, and the effect of input correlations, as a function of all system parameters including the delay.

In contrast, the goal of our contribution is to extend the two-state transition formalism, developed originally in the area of population dynamics and recently applied to neural networks, to the non-Markovian case with delay. The interest in that formalism is its convergence to the well-known population rate formalism of Wilson-Cowan in the infinite size limit (which is also used in neural field theory). This formalism of course gives up some of the biophysical detail of LIF models. But nevertheless, it accurately explains many network phenomena, including finite-size effects that drive oscillations and find their source in the single-neuron probabilistic transitions. We show that this formalism provides a comparatively simple method to compute the basic spectral properties of networks with delay illustrated here on a globally connected inhibitory network. It does not need the time-dependent Fokker Planck formalism for LIF neurons, but rather derives nonlinear rate equations with multiplicative Gaussian white noise (which originate in the Poisson firing statistics). Further, this formalism provides simple nonlinear stochastic delay-differential equations that can be simulated directly to obtain spectral features in all regimes, which is much faster than full network simulations. These can be further analyzed to produce, as we have shown, relatively simple analytic expressions for the power below and near the Hopf bifurcation.

We should emphasize as well that even though the theoretical spectrum fails above the bifurcation, spectra computed from much faster simulations of the stochastic DDE (or SDDE) (2) (compared to full network simulations) provide an accurate description in all regimes investigated. It can thus serve as a simple realistic "model of the full model." The analysis of the strong yet sporadic phase fluctuations that our Hilbert analysis revealed based on full network simulations could also be analyzed quickly using this simplified SDDE.

There are a number of possible extensions to this work. First, instead of focusing on the interneurons, one can analyze an E-E network of pyramidal cells with delays. It could also be extended to a PING network with delays. It has been noted in [7], utilizing analytical as well as numerical arguments, that an excitatory network with intrinsic noise but without delays will exhibit stochastic transitions between a high and a low activity. In this E-E case, however, LNA does not apply, as it requires only a single stable steady state for the deterministic system. It is possible then that the analysis in [7] can be generalized to the delay case. We note that [32] applied a delayed master equation to analyze the complex state transitions in a bistable system with delayed feedback driven by noise. Nonetheless, to our knowledge no investigation of this phenomenon has been carried in a neuroscience context.

Also, recently (see [31]) the stochastic transition between different attractors has been studied for an excitatory-inhibitory network. Again, the role of the conduction delay has not been investigated and can be another direction of interest. Finally, it would be interesting to see whether higher-order approximations would enable the theory to work better near or beyond the bifurcation threshold.

ACKNOWLEDGMENTS

A.L. wishes to thank NSERC and the University of Ottawa for funding this project. G.N. thanks CIHR (Canadian Institute of Health Research), the Michael Smith Foundation's EJLB–Michael Smith Chair program, and the Hope for Depression Research Foundation (HDRF) for support.

APPENDIX

1. Stochastic rate model

To clarify the dynamics of the stochastic spiking process, we link the model to a noisy rate equation. To speed up the computational performance of the Markov process in chemical reactions, the τ-leaping formula was introduced in [33,34]; see also [35] for a more recent review. It is common nowadays to use this formula to derive a stochastic differential equation [6,21,22]. This is done in spite of seemingly contradictory requirements, namely that the time step be small in order to take the infinitesimal limit, and large enough to approximate the Poisson distribution by a Gaussian distribution. The derivation of the stochastic differential equation, therefore, is approximate, but it is correct in the deterministic limit corresponding to an infinite size [22].

Let $l(t)$ denote the number of active neurons at time t. We write the evolution of the number of active neurons as a Poisson process,

$$l(t+dt) \simeq l(t) - \mathcal{P}[\alpha l(t)dt] + \mathcal{P}\{[N-l(t)]\beta f[s(t)]dt\},$$

with $\mathcal{P}$ the Poisson distribution. Using the result in probability theory that a Poisson random variable may be approximated by a normal random variable,

$$\mathcal{P}(\mu) \simeq \mathcal{N}(\mu,\mu),$$

where $\mathcal{N}$ is the normal distribution, we get the expression

$$\begin{aligned} l(t+dt) \simeq\ & l(t) - \mathcal{N}(\alpha l(t)dt, \alpha l(t)dt) \\ & + \mathcal{N}([N-l(t)]\beta f[s(t)]dt, [N-l(t)]\beta f[s(t)]dt), \end{aligned}$$

and with the help of

$$\mathcal{N}(\mu,\sigma^2) = \mu + \sigma\mathcal{N}(0,1),$$

we obtain

$$\begin{aligned} l(t+dt) \simeq\ & l(t) - \alpha l(t)dt \\ & + [N-l(t)]\beta f[s(t)]dt \\ & + \sqrt{\alpha l(t)dt + [N-l(t)]\beta f[s(t)]dt}\,\mathcal{N}(0,1). \end{aligned}$$

Introducing finally the variable $r(t) = \frac{l(t)}{N}$ and taking the limit when dt goes to zero, one obtains the nonlinear stochastic DDE,

$$\begin{aligned} \frac{d}{dt}r(t) =\ & -\alpha r(t) + [1-r(t)]\beta f[s(t)] \\ & + \sqrt{\frac{\alpha r(t) + [1-r(t)]\beta f[s(t)]}{N}}\eta(t), \end{aligned} \tag{A1}$$

where η is a Gaussian white noise,

$$\langle \eta(t) \rangle = 0, \quad \langle \eta(t)\eta(t') \rangle = \delta(t-t'),$$

and $s(t)$ the synaptic input given by

$$s(t) = h - wr(t-\tau).$$

2. Linear noise approximation (LNA)

To study (A1), we use the LNA to separate the deterministic and stochastic dynamics. In our situation, the LNA states that the number of active neurons can be approximated by the sum of a deterministic and a stochastic process. Furthermore, the fluctuation part is scaled by a $1/\sqrt{N}$ factor that comes from the Van Kampen system size expansion. More specifically,

$$r(t) = r_0(t) + \frac{1}{\sqrt{N}}\xi(t) + O\left(\frac{1}{N}\right), \tag{A2}$$

with $r_0(t)$ the deterministic part and $\xi(t)$ the stochastic part. The deterministic part obeys the exact rate model,

$$\frac{d}{dt}r_0(t) = -\alpha r_0(t) + [1-r_0(t)]\beta f[s_0(t)], \tag{A3}$$

with the synaptic current given by

$$s_0(t) = h - wr_0(t-\tau).$$

After algebraic computations with a linearization that keeps only the first-order term in $1/\sqrt{N}$, we found that the fluctuation part obeys the linear stochastic DDE,

$$\begin{aligned} \frac{d}{dt}\xi(t) =\ & -\alpha\xi(t) - \beta f[s_0(t)]\xi(t) \\ & - [1-r_0(t)]\beta f'[s_0(t)]w\xi(t-\tau) \\ & + \sqrt{\alpha r_0(t) + [1-r_0(t)]\beta f[s_0(t)]}\eta(t), \end{aligned} \tag{A4}$$

where $\eta(t)$ is again a white noise. Note that in this paper we adopt the Ito convention of stochastic calculus. Note also that the coefficients of the DDE (A4) depend on the solution of the deterministic equation (A3). From (A3), the only stationary state is given by

$$\alpha\bar{r}_0 = (1-\bar{r}_0)\beta f(\bar{s}_0), \tag{A5}$$

where $\bar{s}_0$ is the stationary synaptic input,

$$\bar{s}_0 = h - w\bar{r}_0.$$

The stationary state is illustrated in the first plot of Fig. 8.

3. Stability of the deterministic part

The stability of the stationary state can be studied in the standard way. We expand the solution of the deterministic process around its stationary state,

$$r_0(t) = \bar{r}_0 + \varepsilon r_1(t) + o(\varepsilon^2).$$

Plugging this last expression in (A3) and keeping only the first-order term in ε, we get that the perturbation $r_1(t)$ follows

$$\begin{aligned} \frac{d}{dt}r_1(t) =\ & -\alpha r_1(t) - \beta f(\bar{s}_0)r_1(t) \\ & - w\alpha\bar{r}_0[1-f(\bar{s}_0)]r_1(t-\tau), \end{aligned}$$

where we have used the relation

$$f'(s) = f(s)[1-f(s)].$$

Looking for a solution of the form $r_1(t) = r_1 e^{\lambda t}$, we find that the eigenvalues λ_k are solutions of the characteristic equation

$$\mathcal{C}(\lambda) = \alpha + \beta f(\bar{s}_0) + \lambda + w\alpha\bar{r}_0[1 - f(\bar{s}_0)]e^{-\lambda\tau}.$$

Writing the eigenvalue in the form

$$\lambda = \mu + i\omega,$$

we obtain

$$\alpha + \beta f(\bar{s}_0) + \mu + w\alpha\bar{r}_0[1 - f(\bar{s}_0)]e^{-\mu\tau}\cos\omega\tau = 0,$$

$$\omega - w\alpha\bar{r}_0[1 - f(\bar{s}_0)]e^{-\mu\tau}\sin\omega\tau = 0.$$

One should not confuse the frequency ω and feedback weight w in the latter formula. These two equations were solved simultaneously using the root finder "fsolve" in MATLAB. Because there is an infinite (though countable) number of conjugate pairs of eigenvalues, only the rightmost pairs are displayed. Their determination required many different initial conditions for the root solver. The stationary state is stable when all the eigenvalues have a negative real part ($\mu < 0$). We show in Fig. 7 the eigenvalues for a range of parameters. In Fig. 8, we show the boundary between the stability region (non oscillatory) and the instability region. The black curve is given by simultaneous solutions of these two equations when $\mu = 0$.

4. Power spectrum of the stochastic part

We assume that the deterministic part of the rate model (A3) tends toward its equilibrium (below the threshold of instability). Then, discarding the transient dynamics, the stochastic differential equation (A4) reads

$$\frac{d}{dt}\xi(t) = -\alpha\xi(t) - \beta f(\bar{s}_0)\xi(t) - w\alpha\bar{r}_0[1 - f(\bar{s}_0)]\xi(t-\tau) + \sqrt{2\alpha\bar{r}_0}\eta(t).$$

Using mathematical tools similar to those in [6] for the stochastic Wilson-Cowan model, we can compute the power spectrum of the solution,

$$P(\omega) := \lim_{T\to\infty} \frac{\langle|\hat{\xi}(\omega)|^2\rangle}{T},$$

where $\hat{\xi}(\omega)$ stands for the Fourier transform of the stochastic process given by

$$\hat{\xi}(\omega) = \int_0^T \xi(t)e^{-i\omega t}dt.$$

After algebraic manipulations, we find that

$$P(\omega) = \frac{2\alpha\bar{r}_0}{|\,\alpha + \beta f(\bar{s}_0) + i\omega + w\alpha\bar{r}_0[1 - f(\bar{s}_0)]e^{-i\omega\tau}\,|^2}, \tag{A6}$$

where $\bar{r}_0$ and $\bar{s}_0$ are, respectively, the stationary activity and the stationary synaptic input, both of them given by the deterministic part (A5). Again, one should not confuse ω and w in the formula. The latter formula can be written as

$$P(\omega) = \frac{2\alpha\bar{r}_0}{(\alpha + \beta f(\bar{s}_0) + w\alpha\bar{r}_0[1 - f(\bar{s}_0)\cos\omega\tau]^2) + (\omega - w\alpha\bar{r}_0[1 - f(\bar{s}_0)\sin\omega\tau]^2)}.$$

From the theoretical formula of the power spectrum (A6), a straightforward computation gives us the basic properties

$$\lim_{\omega\to 0} P(\omega) = \frac{2\alpha\bar{r}_0}{|\,\alpha + \beta f(\bar{s}_0) + w\alpha\bar{r}_0[1 - f(\bar{s}_0)]\,|^2}$$

and

$$\lim_{\omega\to\infty} P(\omega) = \frac{\alpha\bar{r}_0}{\omega^2}.$$

In principle, one can differentiate the expression for the power spectrum to obtain the frequency of the main and secondary resonance peaks. After algebraic manipulations, we find that the local extrema are solutions of the nonlinear equation

$$\frac{\omega}{\alpha + \beta f(\bar{s}_0)} = -\tan\omega\tau.$$

From (A2) one obtains (under the assumption that the steady state is stable) the power spectrum $S(\omega)$ of the activity,

$$S(\omega) = 2\pi\bar{r}_0^2\delta(\omega) + \frac{P(\omega)}{N}.$$

The latter formula was given by (5) and compared with stochastic simulation of the full model in Fig. 9.

[1] L. Abbott, K. Rajan, and H. Sompolinksy, *The Dynamic Brain: An Exploration of Neuronal Variability and Its Functional Significance* (Oxford University Press, New York, 2011).

[2] M. M. Churchland and L. F. Abbott, Nat. Neurosci. **15**, 1472 (2012).

[3] A. A. Faisal, L. P. Selen, and D. Wolpert, Nat. Rev. Neurosci. **9**, 292 (2008).

[4] B. Lindner, B. Doiron, and A. Longtin, Phys. Rev. E **72**, 061919 (2005).

[5] R. Zillmer, N. Brunel, and D. Hansel, Phys. Rev. E **79**, 031909 (2009).

[6] E. Wallace, M. Benayoun, W. van Drongelen, and J. D. Cowan, Plos one **6**, e14804 (2011).

[7] P. C. Bressloff, SIAM J. Appl. Math. **70**, 1488 (2009).

[8] A. J. McKane and T. J. Newman, Phys. Rev. Lett. **94**, 218102 (2005).

[9] D. Alonso, A. J. McKane, and M. Pascual, J. R. Soc. Interface **4**, 575 (2007).

[10] M. S. Kukjin Kang, J. A. Henrie, and R. Shapley, J. Comput. Neurosci. **29**, 495 (2010).
[11] G. Buzsáki and X.-J. Wang, Annu. Rev. Neurosci. **35**, 203 (2012).
[12] G. Dumont and J. Henry, J. Math. Biol. **67**, 453 (2013).
[13] G. Dumont and J. Henry, Bull. Math. Biol. **75**, 629 (2013).
[14] M. J. Cáceres, J. A. Carrillo, and B. Perthame, J. Math. Neurosci. **1**, 8567 (2011).
[15] N. Brunel and V. Hakim, Neural Computat. **11**, 1621 (1999).
[16] K. M. Stiefel, B. Englitz, and T. J. Sejnowski, Proc. Natl. Acad. Sci. (USA) **110**, 7886 (2013).
[17] T. Erneux, *Applied Delay Differential Equations*, Surveys and Tutorials in the Applied Mathematical Sciences (Springer, Berlin, 2009), Vol. 3.
[18] M. M. Klosek and R. Kuske, SIAM Multiscale Model. Simul. **3**, 706 (2005).
[19] A. Longtin, J. Milton, J. Bos, and M. Mackey, Phys. Rev. A **41**, 6992 (1990).
[20] B. Ermentrout and D. Terman, *Mathematical Foundations of Neuroscience* (Springer, Berlin, 2010).
[21] E. Wallace, arXiv:1004.4280.
[22] E. Wallace, D. T. Gillespie, K. R. Sanft, and L. R. Petzold (unpublished).
[23] M. A. Buice and J. D. Cowan, Phys. Rev. E **75**, 051919 (2007).
[24] M. Benayoun, J. D. Cowan, W. van Drongelen, and E. Wallace, Plos Computat. Biol. **6**, e1000846 (2010).
[25] P. C. Bressloff and Y. M. Lai, J. Math. Neurosci. **1**, 2 (2011).
[26] H. A. Swadlow and S. G. Waxman, Scholarpedia **7**, 1451 (2012).
[27] B. Boashash, Proc. IEEE **80**, 540 (1992).
[28] D. Nikolić, P. Fries, and W. Singer, Trends Cogn. Sci. **17**, 54 (2013).
[29] P. C. Bressloff, Phys. Rev. E **82**, 051903 (2010).
[30] M. A. Buice and C. C. Chow, Plos Computat. Biol. **9**, e1002872 (2013).
[31] P. C. Bressloff and J. M. Newby, SIAM J. Appl. Dyn. Syst. **12**, 1394 (2013).
[32] L. S. Tsimring and A. Pikovsky, Phys. Rev. Lett. **87**, 250602 (2001).
[33] D. T. Gillespie, Annu. Rev. Phys. Chem. **58**, 35 (2007).
[34] D. T. Gillespie, J. Chem. Phys. **113**, 297 (2000).
[35] D. T. Gillespie, J. Chem. Phys. **115**, 1716 (2001).